Supplemental Information

Supplemental Figures

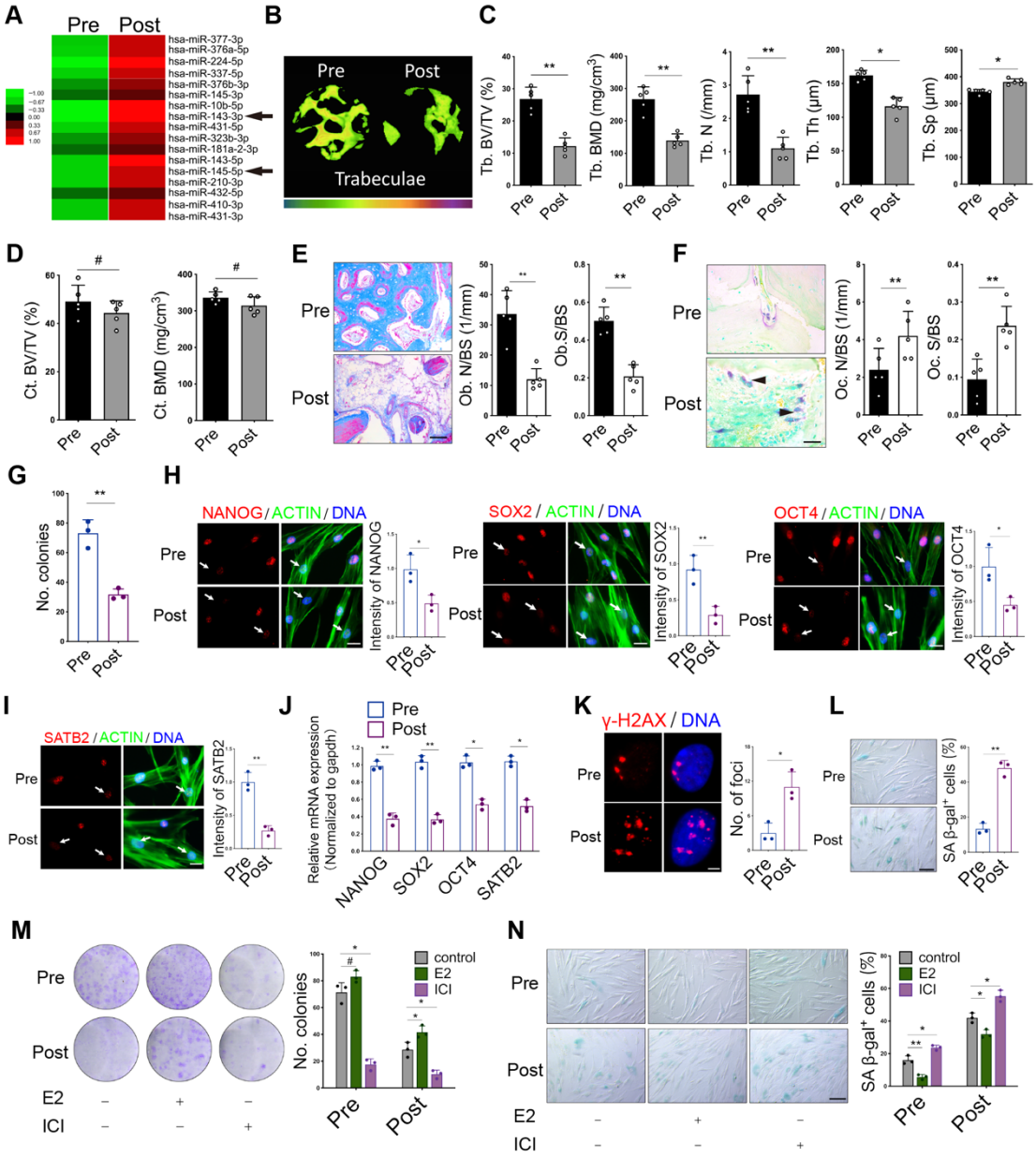

Fig. 1. Increases in miR-143/145 levels during estrogen-deficient osteoporosis and the attenuation of BMSC function

A Heatmap analysis of the miRNAs profiling in Pre- and Post-BMSCs. **B** The trabecular thickness in cancellous bone was color coded, which blue-green color indicates thinner trabeculae and yellow-red color indicates thicker trabeculae. **C** Quantitative measurements of Tb. BV/TV, Tb. BMD Tb. N, Tb. Sp, and Tb. Th of trabeculae were calculated. **D** Cortical bone from dental implantation surgery was quantified for Ct. BV/TV and BMD analysis. **E** Representative masson trichrome

staining images and quantitative for Ob.N/BS and Ob.S/BS analysis were showed. Scale bars: 200 μm. **F** Representative TRAP staining images and quantification of N.Oc/BS (osteoclast number / bone surface). Arrow head indicated the positive staining osteoclasts. Scale bars: 50 μm. **G** The quantification of colonies was analyzed in Pre- and Post-BMSCs. **H, I** Immunostaining of NANOG, SOX2, OCT4 and SATB2 expression in BMSCs. White arrows indicated the BMSCs with decreased core TFs and the mean intensity was measured with ImageJ. Scale bars: 50 μm. **J** qRT-PCR showing NANOG, SOX2, OCT4 and SATB2 mRNA expression in Pre- and Post-BMSCs. **K** γH2AX foci and **(L)** SA-β-gal staining was examined to indicate the senescence difference. Right panel showed the analysis of γH2AX foci numbers and SA-β-gal positive cells. Scale bars: 4 μm **(K)**; 100 μm **(L)**. **M** CFU assays showed that estrogen potentiated colony numbers and ICI reduced the colonies in Pre- or Post-BMSCs. **N** BMSCs stimulated with estrogen or ICI were analyzed for senescence state by SA-β-gal staining. Scale bars: 100 μm. Results are presented as the mean ± S.D. *$p < 0.05$; **$p < 0.01$; #$p > 0.05$ by Student's t test and one-way ANOVA.

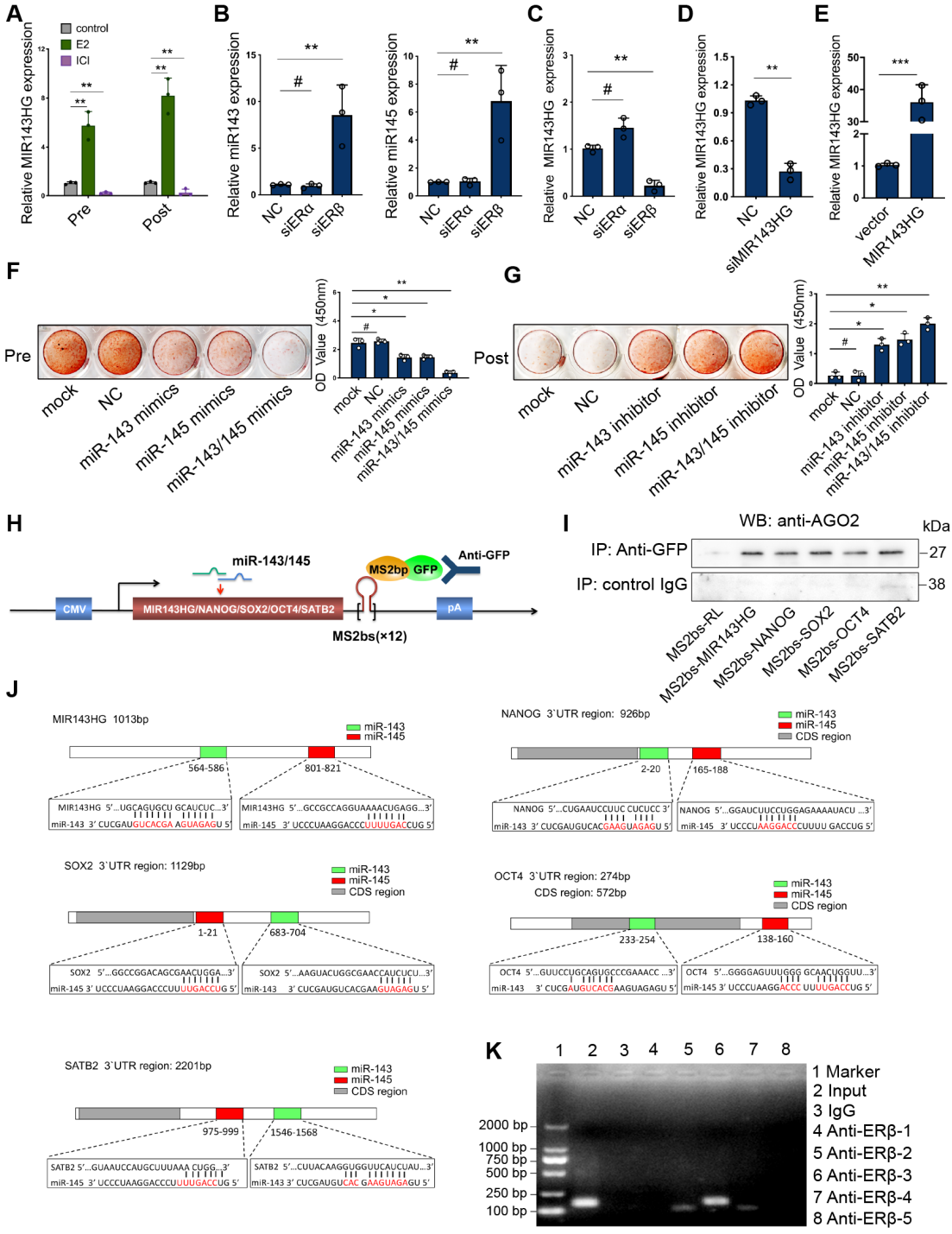

Fig. 2. ERβ activates MIR143HG transcription to regulate the function of miR-143/145 that target core TFs and SATB2

A MIR143HG was detected in estrogen or ICI treated BMSCs. **B, C** qRT-PCR showing the miR-143/145 and MIR143HG expression in siERα or siERβ transfected BMSCs. **D, E** Analysis for knockdown efficiency of MIR143HG siRNA (siMIR143HG) and enhancement efficiency of MIR143HG overexpressing plasmid. **F** Observation and quantitation of calcified nodules formation in Pre BMSCs that transfected with miR-

143/145 mimics by alizarin red staining. **G** Calcified nodules formation and quantitation in Post BMSCs. **H** MS2 system was applied for RIP assay, in which MS2bp specifically binding MS2bs. **I** After precipitated by GFP antibody or IgG, 10% volume of RNA-protein complexes were extracted and subjected to Western blot assay with AGO2 antibody. **J** The putative binding sites of miR-143/145 on MIR143HG, NANOG, SOX2, OCT4 and SATB2 transcripts were predicted by targetscan or Miranda. The red nucleotides indicated the putative paired sites. **K** The amplification products of DNA fragment from ChIP assay were then performed for gel shift assay. E2, estrogen. Results are presented as the mean ± S.D. $*p < 0.05$; $**p < 0.01$; $***p < 0.001$; $\#p > 0.05$ by Student's t test and one-way ANOVA.

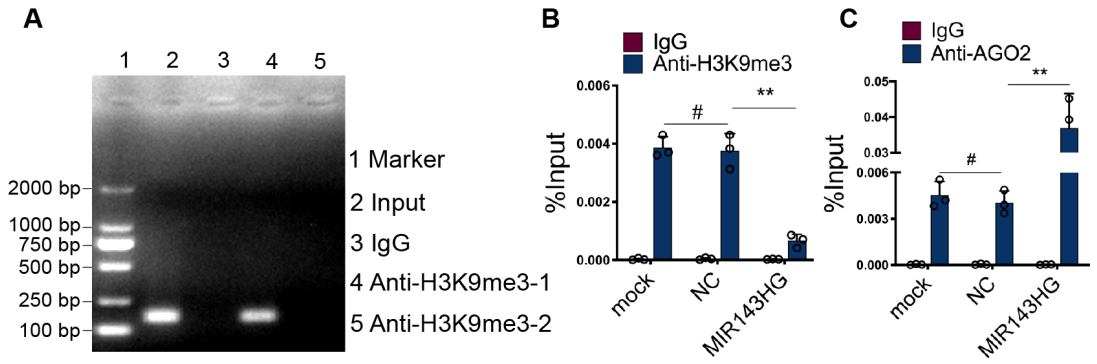

Fig. 3. MIR143HG guides miR-143/145 into nuclear and cooperatively regulates SOX2 transcription

A Amplified DNA using prime 1 or prime 2 were further examined by gel shift assay. **B, C** BMSCs transfected with mock, NC or MIR143HG overexpressing vector were subjected to ChIP assay by H3K9me3 or AGO2 antibody. Results are presented as the mean ± S.D. $^{**}p < 0.01$; $^{\#}p > 0.05$ by Student's t test and one-way ANOVA.

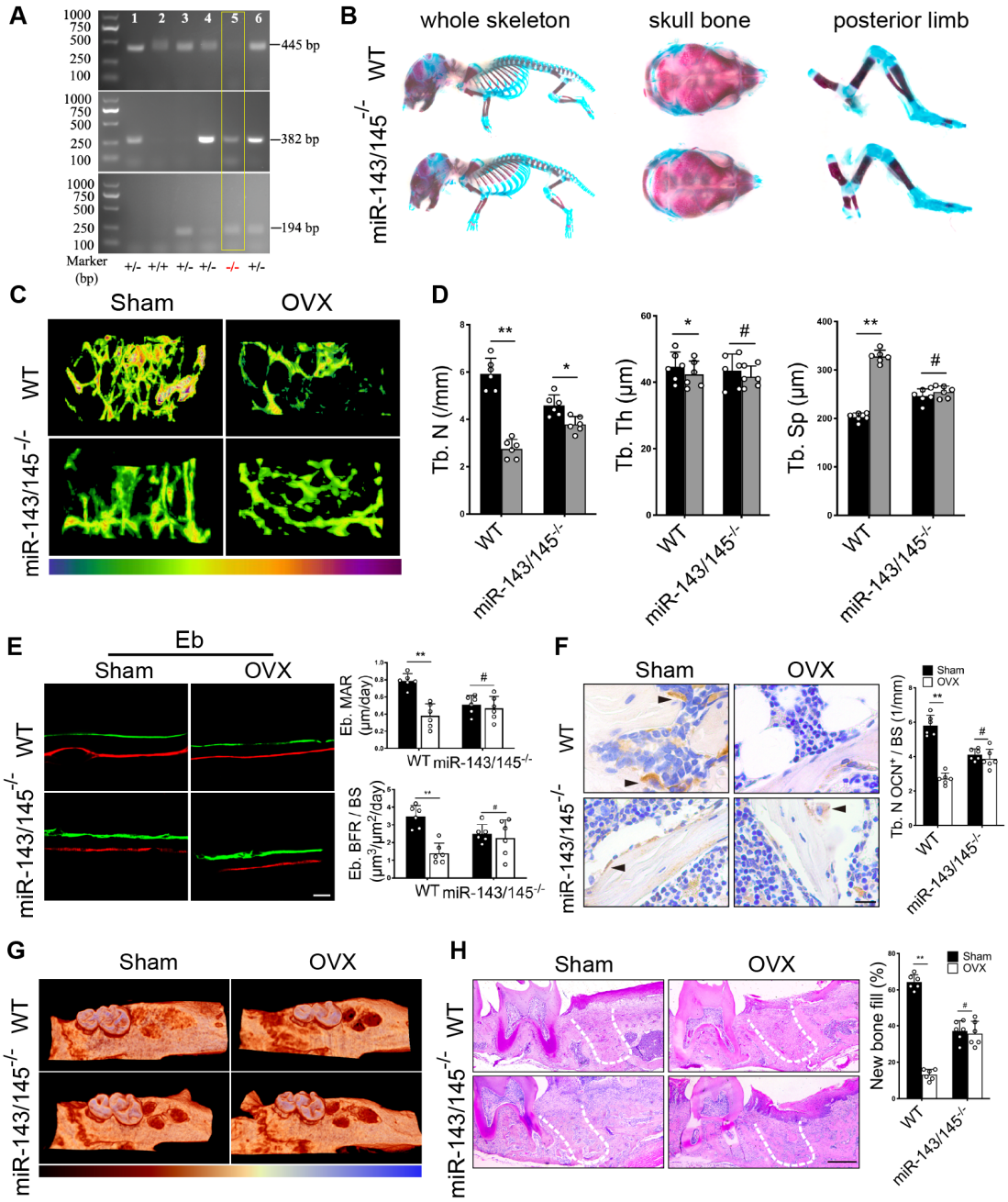

Fig. 4. Depletion of miR-143/145 in mice prevented bone loss and potentiated bone regeneration in OVX-induced osteoporosis

A All mice were genotyped by PCR from tail snip DNA**. B** Whole skeleton staining revealing the whole mount skeleton, skull bone, posterior limb using Alizarin red and Alcian blue. **C** Trabecular thickness maps were presented, which blue-green color indicates thinner trabeculae and yellow-red color indicates thicker trabeculae. **D** Quantitative measurements of Tb. N, Tb. Sp, Tb. Th. **E** Representative images of dynamic histomorphometry of endosteal (Eb) bone with quantification of mineralization apposition rate (MAR) and bone formation rate per bone surface (BFR/BS). Scale bars: 20 μm. **F** Representative OCN positive osteoblasts and

quantification on the trabecular by IHC. Scale bars: 50 μm. **G** Micro-CT analysis of new bone fill in tooth extraction socket by color coded thickness maps. Color changes from red to blue denote a gradual elevation in bone thickness. **H** Representative HE staining showing the new bone mass and quantification of new bone fill in tooth extraction socket, which was delineated by white dotted lines. Scale bars: 100 μm. Results are presented as the mean ± S.D. *$p < 0.05$; **$p < 0.01$; ***$p < 0.001$; #$p > 0.05$ by two-way ANOVA, n = 6 mice per group.

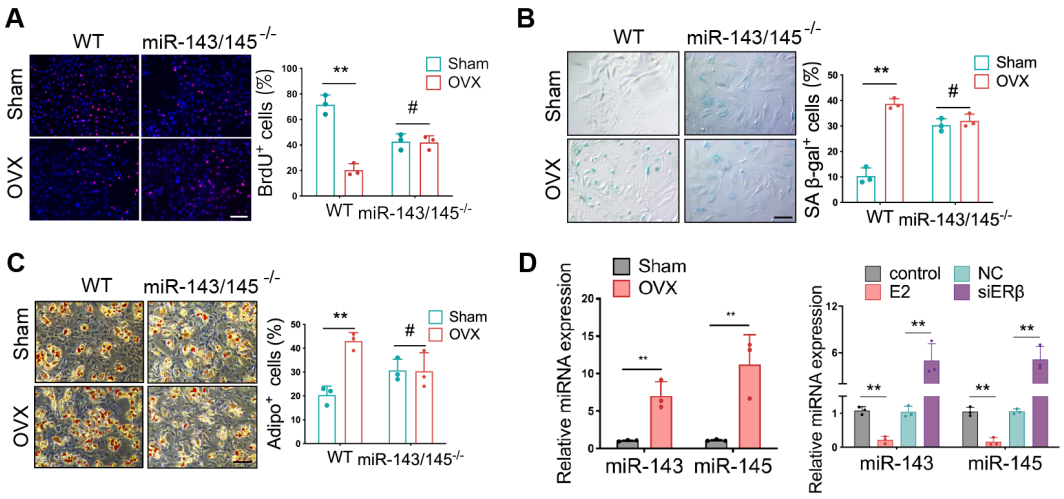

Fig. 5. miR-143/145 depletion counteracts the adverse effects of estrogen deficiency on BMSCs function

A BrdU assay revealing proliferation ability in Sham and OVX-induced WT and *miR-143/145*$^{-/-}$ BMSCs. Scale bars: 100 μm. **B** SA-β-gal showing the senescence difference in WT and *miR-143/145*$^{-/-}$ BMSCs following OVX. Right panel shows the respective quantification. Scale bars: 100 μm. **C** Oil red O staining showing the ability of adipogenic differentiation. Right panel shows the respective quantification. Scale bars: 100 μm. **D** Detection of miR-143/145 in OVX BMSCs and estrogen or siERβ treated BMSCs. Results are presented as the mean ± S.D. *$p < 0.05$; **$p < 0.01$ by Student's t test and one-way ANOVA.

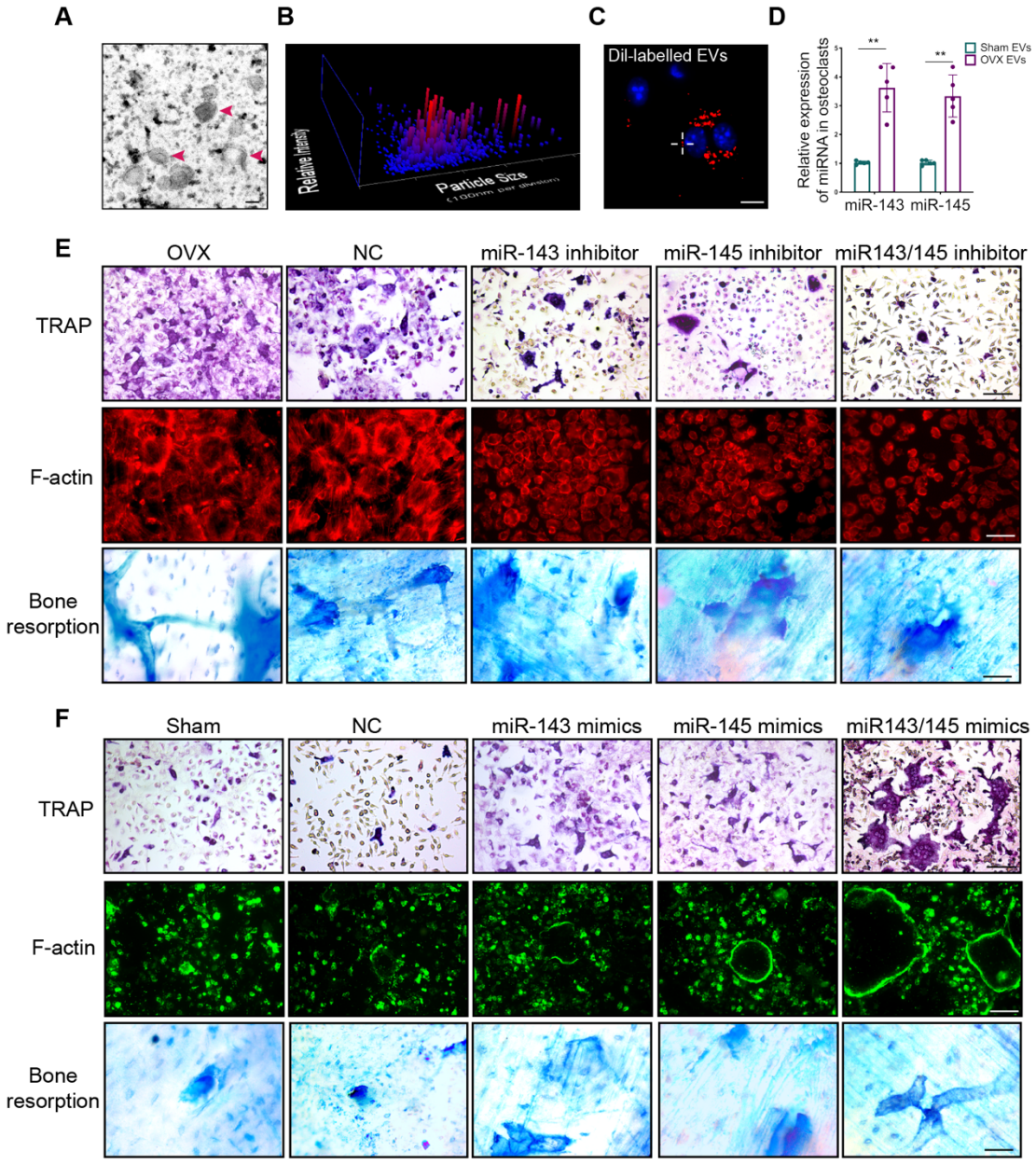

Fig. 6. EVs loaded miR-143/145 from BMSCs activates osteoclast function

A An overview TEM image of EVs that indicated by red arrows were captured to understand the whole EVs population. Scale bars: 100 nm. **B** The 3D graph (particle size vs. Relative intensity vs. particle number concentration) of NTA for calculating EVs size distribution. **C** Fluorescent microscopy analysis revealing the DiI-labeled EVs incorporated into osteoclasts. Scale bars: 50 μm **(C)**. **D** Osteoclasts co-cultured with EVs from Sham or OVX-induced BMSCs were examined by qRT-PCR. **E, F** Representative images of TRAP positive staining, F-actin ring staining, and bone resorption area in miR-143/145 inhibitor or mimics treated osteoclasts. Scale bars: 100 μm **(E, F)**. Results are presented as the mean ± S.D. *$p < 0.05$; **$p < 0.01$ by Student's t test.

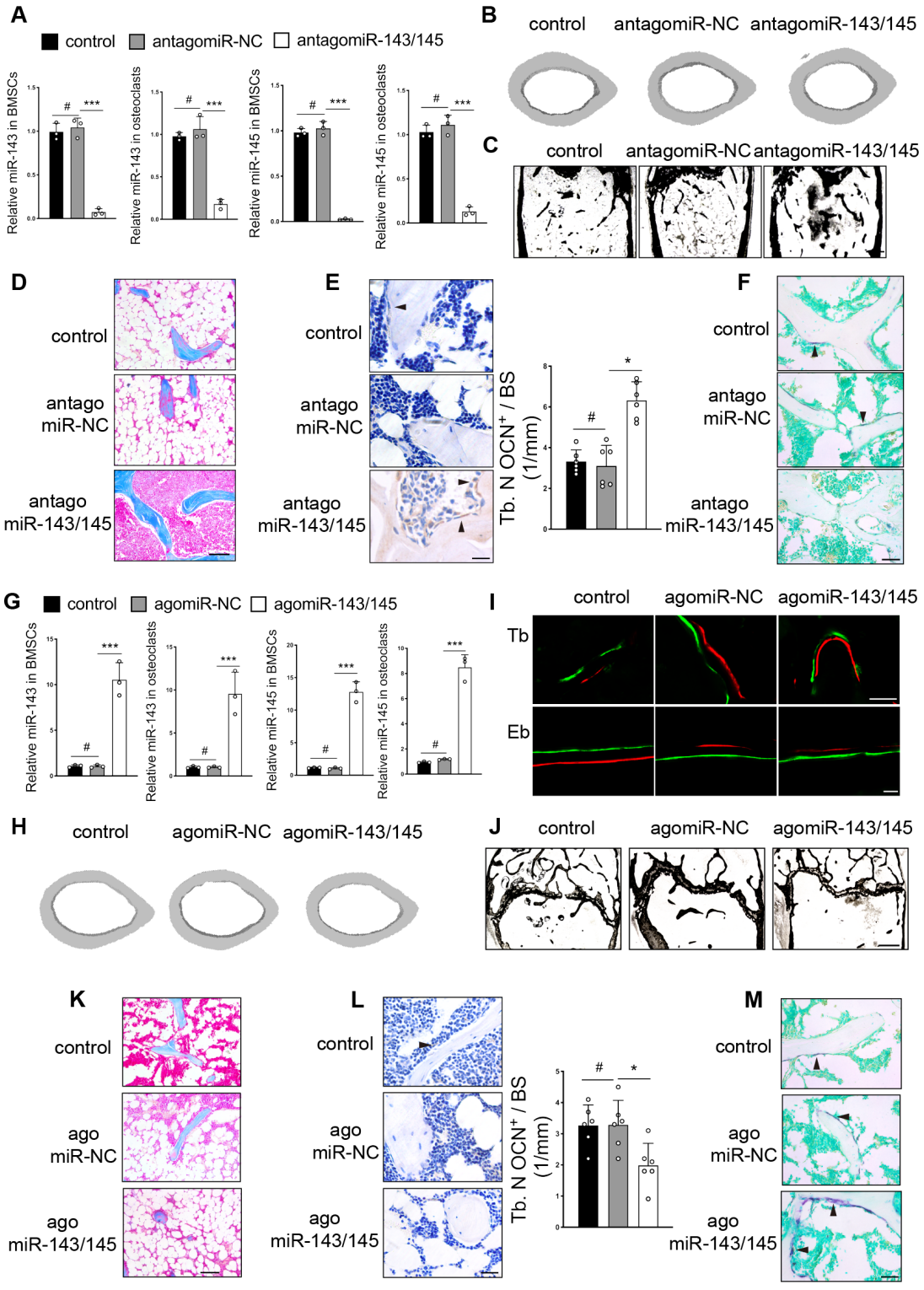

Fig. 7. AntagomiR-143/145 prevents and agomiR-143/145 exacerbates OVX-induced bone loss

A qRT-PCR analysis of miR-143/145 expression in BMSCs and osteoclasts of mice with antagomiR. **B** Representative micro-CT images of cortical bone from control, antagomiR-NC, and antagomiR-143/145 treated femurs. **C** Von Kossa staining showing

an overall trabecular bone mass. Scale bars: 500 μm. **D** Masson trichrome staining revealing the trabecular bone accounts. Scale bars: 100 μm. **E** IHC showing the OCN positive osteoblasts. Arrow head indicated the positive staining osteoblasts. Scale bars: 50 μm. **F** TRAP staining showing osteoclastic activity. Arrow head indicated the positive staining osteoclasts. Scale bars: 50 μm. **G** qRT-PCR analysis of miR-143/145 expression in BMSCs and osteoclasts with agomiR. **H** Micro-CT images of cortical bone from control, agomiR-NC, and agomiR-143/145 treated mice. **I** Representative images of dynamic histomorphometry of Tb and Eb bone. Scale bars: 20 μm. **J** Representative images of von Kossa showing an overall trabecular bone mass. Scale bars: 500 μm. **K** Representative images of masson trichrome staining revealing the trabecular bone mass and quantification of osteoblast numbers and surface on the trabecular, **(L)** as well as OCN positive osteoblasts by IHC. Scale bars: 100 μm **(K)**; 50 μm **(L)**. Arrow head indicated the positive staining osteoblasts. **M** Representative images of TRAP staining showing osteoclastic activity. Arrow head indicated the positive staining osteoclasts. Scale bars: 50 μm. Results are presented as the mean ± S.D. *$p < 0.05$; #$p > 0.05$, by one-way ANOVA, n = 6 mice per group.

Supplemental Table

Table S1. Primer sequence for qRT-PCR and ChIP qPCR.

Gene	Primer Sequence
Primer for human GAPDH	F 5′-GGAGATTACTGCCCTGGCTCCTA-3′
	R 5′-GACTCATCGTACTCCTGCTTGCTG-3′
Primer for human NANOG	F 5′-AAGGTCCCGGTCAAGAAACAG-3′
	R 5′-CTTCTGCGTCACACCATTGC-3′
Primer for human SOX2	F 5′-GGCAGAGAAGAGAGTGTTTGC-3′
	R 5′-GCCGCCGATGATTGTTATT-3′
Primer for human OCT4	F 5′-TGAGAGGCAACCTGGAGAAT-3′
	R 5′-AACCACACTCGGACCACATC-3′
Primer for human SATB2	F 5′-CCAGGAGTTTGGGAGATGGTAT-3′
	R 5′-GTGAGGAGACTGTTCGTTGGTT-3′
Primer for human MIR143HG	F 5′-AGAGCCGCCAGGTAAAAC-3′
	R 5′-TCCAACCCCACCAAAGG-3′
Primer for mouse pri-miR-143	F5′-GTCTCCAGGGCGTGTCCAGACCAGTA-
	R 5′ CCTGAGCTACAGTGCTTCATCTCAGA-3′
Primer for mouse pri-miR-145	F 5′-GTCCAGTTTTCCCAGGAATCCCTT-3′
	R 5′ GTCCCAAGACCGCTTACCTCCCTC-3′
Primer for human MIR143HG Promotor-1 (ChIP-ERβ)	F 5′-TGAGTCATAGCTTACATC-3′
	R 5′-GGAACTAACTTCTGTGAA-3′
	F 5′-CCACTCAGGATGTCACAAG-3′

Primer for human MIR143HG Promotor-2 (ChIP-ERβ)	R 5′-CTCATTCACAGTTCCTCAGA-3′
Primer for human MIR143HG Promotor-3 (ChIP-ERβ)	F 5′-CTCTGGGAAGAAGGCATTT-3′
	R 5′-GGGTTTGAATGTGGAATGTC-3′
Primer for human MIR143HG Promotor-4 (ChIP-ERβ)	F 5′-CCTGAAGGACATTCCACAT-3′
	R 5′-GAAGCTACTCCCATCATCAT-3′
Primer for human MIR143HG Promotor-5 (ChIP-ERβ)	F 5′-TCTCAGGCTTAATGACTTC-3′
	R 5′-AAGGAGTGGTTGACAATT-3′
Primer for human SOX2 Promotor-1 (ChIP-RNAa complex)	F 5′-AAGGTTAGTAAGGAACAA-3′
	R 5′-TTCTTCTGTAACACTCTC-3′
Primer for human SOX2 Promotor-2 (ChIP-RNAa complex)	F 5′-TGTAGCGACAACAAGAGAA-3′
	R 5′-GTTAGAGGAGGATGAGATGG-3′
Primer for mouse miR-143/145 Promotor (ChIP-ERβ)	F 5′-AGGGACCCCAAATCATAA-3′
	R 5′-AACCTACCTCATCCTCTG-3′

Table S2. Information of Antibodies, Chemicals Reagent, Commercial Kit, Cell Lines, mouse Strains, Recombinant DNA and Software in this study.

REAGENT or RESOURCE	SOURCE	Cat#
Antibodies (Dilution)		
Rabbit polyclonal anti-NANOG (1:500)	Santa Cruz	Cat# sc-33760
Rabbit monoclonal anti-SOX2 (1:1000)	Abcam	Cat# ab93689
Rabbit monoclonal anti-OCT4 (1:1000)	Abcam	Cat# ab181557
Rabbit polyclonal anti-SATB2 (1:1000)	Abcam	Cat# ab69995
Mouse monoclonal anti-BrdU (1:500)	Proteintech	Cat# MS-396-P1
Mouse monoclonal anti-γH2AX (1:1000)	Abcam	Cat# ab26350
Rabbit polyclonal anti-P53 (1:800)	Proteintech	Cat# 10442-1-AP
Rabbit polyclonal anti-P21 (1:500)	Proteintech	Cat# 10355-1-AP
Rabbit polyclonal anti-GFP (1:1000)	Abcam	Cat# ab290
Rabbit monoclonal anti-AGO2 (1:1000)	Cell Signaling Technology	Cat# 2897
Rabbit polyclonal anti-H3K9me3 (1:1000)	Abcam	Cat# ab8898
Mouse monoclonal anti-LMNA (1:1000)	Cell Signaling Technology	Cat# 86846
Rabbit polyclonal anti- RUNX2 (1:1000)	Cell Signaling Technology	Cat# AP12556PU-N
Rabbit polyclonal anti-OCN (1:1000)	Abcam	Cat# ab93876
Rabbit polyclonal anti-CD226 (1:500)	Affinity Bioscience	Cat# AF0087
Rabbit Polyclonal anti-SRGAP2 (1:500)	Proteintech	Cat# 22519-1-AP
Mouse monoclonal anti-CD63 (1:1000)	Abcam	Cat# ab213090
Rabbit monoclonal anti-CD9 (1:1000)	Abcam	Cat# ab92726
Rabbit Polyclonal anti-Estrogen Receptor beta (1:1000)	Abcam	Cat# ab3577

Chemicals, Peptides, and Recombinant Proteins		
DMEM, low glucose	Thermo Fisher Scientific	Cat# 11885084
MEM Alpha basic	Thermo Fisher Scientific	Cat# 12571063
Fetal Bovine Serum	Thermo Fisher Scientific	Cat# 16140071
Penicillin-Streptomycin	Sigma-Aldrich	Cat# V900929
Red Blood Cell Lysis Buffer	Beyotime	Cat# C3702
Estrogen	Sigma-Aldrich	Cat# 1250008
Estrogen Receptor Antagonist, ICI 182,780	Sigma-Aldrich	Cat# 5. 31042
L-Ascorbic acid	Sigma-Aldrich	Cat# A5960
β-Glycerophosphate	Sigma-Aldrich	Cat# E2758
dexamethasone	Sigma-Aldrich	Cat# D4902
Insulins	Sigma-Aldrich	Cat# I0908
3-isobutyl-1-methylxanthine	Sigma-Aldrich	Cat# I5879
Indomethacin	Sigma-Aldrich	Cat# I7378
Oil Red O	Sigma-Aldrich	Cat# O0625
Anti-Murine M-CSF	PeproTech	Cat# 500-P62G
Recombinant Murine sRANK Ligand	PeproTech	Cat# 315-11
Lipofectamine™ 2000 Transfection Reagent	Invitrogen	Cat# 11668027
TRIzol™ LS Reagent	Invitrogen	Cat# 10296010
Calcein	Sigma-Aldrich	Cat# C0875
Alizarin Red S	Sigma-Aldrich	Cat# A5533
DiIC18(3) (Ex/Em:550/567nm)	YEASEN	Cat# 40726ES10

Critical Commercial Assays		
miRNeasy Serum/Plasma kit	QIAGEN	Cat# 217184
TRAP staining kit	Sigma-Aldrich	Cat# N2250
β-Gal Staining Kit	GenMed	Cat# GMS10012.1
All-in-One miRNA qRT-PCR Detection Kit	GeneCopoeia	Cat# QP004
EZ-Magna RIP™ RNA-Binding Protein Immunoprecipitation Kit	Millipore	Cat# 17-701
Hyperactive in-Situ ChIP kit	Vazyme	Cat# TD901-01
Fluorescent in situ hybridization kit	Genepharma	Cat# F03201
Dual-Luciferase Reporter Assay System	Promega	Cat# E1960
Experimental Models: Cell Lines		
Human: alveolar bone marrow-derived mesenchymal stem cells	This paper	N/A
Mouse: bone marrow-derived mesenchymal stem cells	This paper	N/A
Human: 293T cells	ATCC	CM-1009
Experimental Models: Organisms/Strains		
Mouse: miR-143/145$^{-/-}$ (B6/N-miR-143/145^{tm1})	Model Animal Research Center of Nanjing	T000090
Oligonucleotides		
GMR-miRTM microRNA single-stranded mimics	Genepharma	B01001
GMR-miRTM microRNA inhibitors	Genepharma	B03001
miR-UPTM agomir	Genepharma	B06002
miR-DownTM antagomir	Genepharma	B05002
Chemically modified siRNA	Genepharma	A02004
Recombinant DNA		

Plasmid: pEX-3 (pGCMV/MCS/Neo) vector	Genepharma	N/A
Plasmid: pcDNA3-MS2 system vector	GeneCopoeia	N/A
Plasmid: pGL3-basic luciferase reporter vector	GeneCopoeia	N/A
Software and Algorithms		
ImageJ	Softonic	https://imagej.en.softonic.com/
LAS V4.12	Leica Microsystems	https://www.leica-
GraphPad Prism 8	GraphPad	https://www.graphpad.com/
Micro-CT NRecon v1.6 and CTAn v1.13.8.1	Skyscan	https://www.skyscan.pt/
Image-Pro Plus 7	Media Cybernetics	http://www.mediacy.com/image
Adobe Illustrator	Adobe	https://www.adobe.com/cn/prod